Liufeng Mao,[1] Baoming Nie,[2] Tao Nie,[1] Xiaoyan Hui,[3] Xuefei Gao,[4] Xiaoliang Lin,[5] Xin Liu,[6] Yong Xu,[1] Xiaofeng Tang,[1] Ran Yuan,[1] Kuai Li,[1] Peng Li,[1] Ke Ding,[1] Yu Wang,[1,3] Aimin Xu,[1,3] Jian Fei,[7] Weiping Han,[8] Pentao Liu,[4] Lise Madsen,[9,10,11] Karsten Kristiansen,[10,11] Zhiguang Zhou,[12] Sheng Ding,[2] and Donghai Wu[1,13]

# Visualization and Quantification of Browning Using a *Ucp1*-2A-Luciferase Knock-in Mouse Model

*Diabetes 2017;66:407–417 | DOI: 10.2337/db16-0343*

**Both mammals and adult humans possess classic brown adipocytes and beige adipocytes, and the amount and activity of these adipocytes are considered key factors in combating obesity and its associated metabolic diseases. Uncoupling protein 1 (Ucp1) is the functional marker of both brown and beige adipocytes. To facilitate a reliable, easy, and sensitive measurement of *Ucp1* expression both in vivo and in vitro, we generated a *Ucp1*-2A-luciferase knock-in mouse by deleting the stop codon for the mouse *Ucp1* gene and replacing it with a 2A peptide. This peptide was followed by the luciferase coding sequence to recapitulate the expression of the *Ucp1* gene at the transcriptional and translational levels. With this mouse, we discovered a cold-sensitive brown/beige adipose depot underneath the skin of the ears, which we named uBAT. Because of the sensitivity and high dynamic range of luciferase activity, the *Ucp1*-2A-luciferase mouse is useful for both in vitro quantitative determination and in vivo visualization of nonshivering thermogenesis. With the use of this model, we identified and characterized axitinib, an oral small-molecule tyrosine kinase inhibitor, as an effective browning agent.**

The obesity epidemic has led to intensified efforts to understand adipose tissue development and function. Currently, we know of three kinds of adipocytes: the classic multilocular brown adipocyte in brown adipose tissue (BAT); the classic unilocular white adipocyte, which is the main cell type in white adipose tissue (WAT); and the brite/beige adipocyte in WAT. Although WAT stores excessive energy as fat, brown and brite/beige adipocytes dissipate energy as heat. A number of studies have demonstrated that adult humans possess functional BAT, which can be activated by mild cold exposure (1–3) and treatment with a β3-adrenergic agonist (4). In humans, activation of BAT reduces elevated blood triglycerides and alleviates obesity (5). In mice, BAT transplantation decreases body weight and improves glucose homeostasis and insulin sensitivity in both chow- and high-fat–fed mice (6,7). Therefore, enhancing thermogenic function in BAT and recruiting BAT-like brite/beige adipocytes in WAT may be effective therapeutic strategies for combating obesity and its associated disorders.

The energy-dissipating, thermogenic function of BAT and beige adipocytes is mainly achieved by the uncoupling protein 1 (UCP1). UCP1 is located in the inner mitochondrial

[1]CAS Key Laboratory of Regenerative Biology, Joint School of Life Sciences, Guangzhou Medical University, and Guangzhou Institute of Biomedicine and Health, Chinese Academy of Sciences, Guangzhou, China
[2]Gladstone Institute of Cardiovascular Disease, Department of Pharmaceutical Chemistry, University of California, San Francisco, San Francisco, CA
[3]Department of Medicine, The University of Hong Kong, Hong Kong
[4]Wellcome Sanger Institute, Cambridge, U.K.
[5]Research & Development Center, Infinitus (China) Company Ltd., Guangzhou, China
[6]Shenzhen Institutes of Advanced Technology, Chinese Academy of Sciences, Shenzhen, China
[7]Shanghai Nan Fang Model Organism Research Center, Shanghai, China
[8]Singapore Bioimaging Consortium and Institute of Molecular and Cell Biology, Agency for Science, Technology and Research, Singapore
[9]National Institute of Nutrition and Seafood Research, Bergen, Norway
[10]Laboratory of Genomics and Molecular Biomedicine, Department of Biology, University of Copenhagen, Copenhagen, Denmark
[11]Beijing Genomics Institute-Shenzhen, Shenzhen, China
[12]Diabetes Center, The Second Xiangya Hospital, Institute of Metabolism and Endocrinology, Central South University, Changsha, China
[13]Joint School of Biological Sciences, Guangzhou Institute of Biomedicine and Health, Guangzhou Medical University, Guangzhou, China

Corresponding authors: Donghai Wu, wu_donghai@gibh.ac.cn, and Sheng Ding, sheng.ding@gladstone.ucsf.edu.

Received 15 March 2016 and accepted 31 October 2016.

This article contains Supplementary Data online at http://diabetes.diabetesjournals.org/lookup/suppl/doi:10.2337/db16-0343/-/DC1.

L. Mao, B.N., and T.N. contributed equally to this work.

membrane where it allows protons to flow back into the mitochondria, thereby uncoupling electron transport from ATP production. By enhancing the futile cycle of proton and electron transport, it increases energy expenditure in the form of heat. In this context, increasing UCP1 expression and activity in adipose tissues is regarded as a safe and promising way to enhance whole-body energy expenditure and combat obesity. Under physiological conditions, brown and beige adipocytes readily respond to stimuli such as cold exposure and β3-adrenergic agonists to increase the expression and activity of UCP1. On the other hand, pharmacological administration of cytokines or compounds such as fibroblast growth factor 21 (FGF21), adenosine $A_{2A}$ receptor agonist, and berberine has been demonstrated to enhance energy expenditure through inducing UCP1 expression in BAT or WAT (8–10).

Despite these findings, more efficacious reagents and a detailed understanding of the underlying mechanisms regarding the recruitment and activation of Ucp1-positve adipocytes are still lacking. To gain more insight into this aspect, several transgenic mouse models have been established. UCP1-GFP and UCP1–CreER:ROSA–tdRFP mice were used to transiently or permanently label UCP1-expressing cells in vivo, respectively. Combined usage of these two transgenic mouse models allows for the tracing of current and past UCP1-positive cells to investigate the interconversion of brite/beige adipocytes (11). Galmozzi et al. (12) generated a ThermoMouse where a *Ucp1* promoter–driven luciferase reporter was integrated into the Y chromosome, which restricts the utility of this model to only male mice. To obtain a more comparative and comprehensive understanding of browning in both male and female mice during development and/or disease, a need still exists for a reliable functional readout that monitors metabolic changes in fat pads induced by cold exposure or drugs (11). We report on our generation of *Ucp1*-luciferase reporter mice, our discovery of an unappreciated brite/beige fat pad underneath their ears, and our identification and characterization of an effective agent for browning.

## RESEARCH DESIGN AND METHODS

### Generation of the *Ucp1*-2A-Luciferase Construct

Standard homologous recombination procedures were used to target firefly luciferase following exon 6 of the endogenous *Ucp1* gene. A left arm of 4.3 kb before the stop codon of the *Ucp1* gene, a right arm of 2.5 kb right after the stop codon of the *Ucp1* gene flanking the 2A peptide (GSGATNFSLLKQAGDVEENPGP), and a firefly luciferase coding sequence followed by a floxed neomycin selection cassette were used for the generation of targeted insertion at the *Ucp1* locus. The correct targeted embryonic stem cell (ES) clones were identified and the floxed neomycin cassette removed before they were used in the production of chimeras. The 129 mouse strain was used for the construction of the knock-in mice. The mice were backcrossed with C57BL/6J for 10 generations before their use in this study. The primers used for *Ucp1-Luc* genotyping were as follows: F1, CAACAGCGGGCTCTGCAC; R1, AACCGTAGGTTGCGCA CTC; and R2, CACGGTAGGCTGCGAAATG. The resulting PCR products were 500 (wild type [WT]) and 1,000 (UCP1) base pairs (bp) in length.

### Animal Studies

Male heterozygous Ucp1+/LUC mice (7 weeks old) on a C57BL/6J background were housed in specific pathogen–free mouse rooms, maintained on a 12-h light-dark cycle at 22°C, and fed standard chow (15.9 kJ/g, 10% of energy as fat, 20% of energy as protein, 70% of energy as carbohydrate). For cold challenge experiments, mice were housed at 4°C for 3, 6, 9, or 12 h. For thermoneutrality experiments, mice were housed at 4°C or 22°C for 12 h and then housed at 30°C for 48 h. For drug challenge experiments, mice were given CL316,243 (1 mg/kg) for 2 days, and in vivo luciferase images were taken. Alternatively, mice were fed a high-fat diet (HFD) (21.9 kJ/g, 60% of energy as fat, 20% of energy as protein, 20% of energy as carbohydrate, D12492; Research Diets, New Brunswick, NJ). At the same time, mice were given axitinib (10 mg/kg body weight; Pfizer, Freiburg, Germany) or PBS every day by oral gavage for 8 weeks. Energy expenditure was measured by indirect calorimetry (Columbus Instruments).

### In Vivo, Ex Vivo, and In Vitro Luciferase Imaging

Bioluminescence imaging was performed with an IVIS Imaging System 50 Series (Xenogen Corp.). For in vivo luciferase imaging, mice were injected with 150 mg/kg body weight intraperitoneally (i.p.) D-luciferin solution (Promega). Ten minutes later, mice were anesthetized within a clear Plexiglas anesthesia box (2.5–3.5% isoflurane) for 5 min) and then transferred to nose cones attached to the manifold in the imaging chamber. Because volatile anesthesia, such as isoflurane, is known to inhibit thermogenesis (13), data would represent an underestimate of the true state of thermogenic function. Nonetheless, isoflurane was used because the level of anesthesia is readily controllable and has been commonly used in mice during imaging. The imaging capture time was set between 1 and 5 min per side (dorsal/ventral), depending on the experiment. Luminescence was quantified using Living Image software.

For ex vivo luciferase imaging of various fat depots, the mice were injected with 150 mg/kg body weight i.p. D-luciferin solution for 20 min before fat depots were harvested and luciferase images taken. For in vitro luciferase imaging of the cultured cells, at day 10 of adipogenic differentiation, D-luciferin was added to cell media at a concentration of 150 μg/mL and images captured 10 min later.

### In Vitro Analysis of Luciferase Activity

In vitro luciferase activity was measured by using the Steady-Glo Luciferase Assay System (E2510; Promega) according to the manufacturer's instructions. Cells and mouse tissues were washed twice with ice-cold PBS and lysed with lysis buffer (Promega) for 30 min on ice. Cell lysates were centrifuged at 12,000*g* for 15 min at 4°C, and 20 μL of supernatant and 20 μL of DMEM were mixed with 40 μL of

Steady-Glo reagent in the wells of 96-well solid-bottom white plates (CulturPlate-96, PerkinElmer, North Billerica, MA). The signal was measured with a Veritas Microplate Luminometer (Turner BioSystems, Sunnyvale, CA) and normalized with protein concentrations.

### Isolation and Differentiation of Preadipocytes

Isolation of stromal cells from fat tissue was performed as previously described (8,14,15). Adipose tissues were dissected out, rinsed in PBS, minced, and digested for 40 min at 37°C in 0.1% (weight for volume) collagenase solution (collagenase type I). Digested tissue was filtered through a 100-μm nylon mesh to remove undigested tissues before centrifugation at 1,000*g* for 5 min. The pellets were washed in PBS before seeded in DMEM supplemented with 15% FBS and 1% penicillin/streptomycin.

For differentiation, preadipocytes were cultured in DMEM with 10% FBS. Two days after reaching confluence (day 0), differentiation was induced by differentiation medium containing 5 μg/mL insulin (Sigma), 1 μmol/L dexamethasone (Sigma), and 0.5 mmol/L isobutylmethylxanthine (Sigma). After 2 days, the media were replaced with DMEM supplemented with 10% FBS, 5 μg/mL insulin, and 1 μmol/L rosiglitazone and changed every 2 days until day 8. After that, cells were treated with various compounds in DMEM supplemented with 10% FBS for another 2 days.

### Half-lives of UCP1 and Luciferase

Mature brown adipocytes were treated with CL316,243 for 2 days followed by 10 μmol/L cycloheximide at time point 0 to arrest protein translation. At various time points thereafter, expression of UCP1 and luciferase were examined by Western blotting and luminescence assay, respectively.

### Seahorse Analysis

The oxygen consumption rate (OCR) of the inguinal WAT (ingWAT) cells was analyzed by using the XF24 Seahorse bioanalyzer as previously described with minor modifications (16). Briefly, the cells were treated with axitinib (1 μmol/L) or DMSO 2 days before analysis. Next, the cells were equilibrated in $CO_2$-free DMEM for 1 h in a $CO_2$-free incubator. The following drugs were sequentially loaded to measure basal (vehicle), stimulated (10 μmol/L norepinephrine), ATP production (2 μmol/L oligomycin), maximal [2 μmol/L carbonyl cyanide-4-(trifluoromethoxy)phenylhydrazone], and nonmitochondrial (1 μmol/L antimycin A + 3 μmol/L rotenone) OCRs. Uncoupled OCR was calculated as the difference between stimulated and nonmitochondrial OCRs. Seahorse analyses reportedly may not be performed optimally if the BSA was not present in the medium, which suggests that respiration is not UCP1 dependent (17). However, the mitochondrial content in the cells could be functionally measured by the current procedure.

### Glucose and Insulin Tolerance Tests

For the glucose tolerance test, nine pairs of mice were fasted overnight and injected with 1 g/kg body weight i.p. glucose. For the insulin tolerance test, mice were fasted for 6 h and injected with 0.5 units/kg body weight i.p. recombinant human insulin (Sigma). Blood glucose was monitored with a glucometer (Roche Diagnostics) at various time points.

### Histochemistry and Immunohistochemistry

Adipose tissues were isolated and fixed in 4% formaldehyde overnight. Tissues were paraffinized and sectioned at 5 μm. The sections were stained with hematoxylin-eosin (H-E) (Sigma) according to standard protocol and examined by light microscopy. For immunofluorescence staining, coverslips plated with differentiated adipocytes were fixed in 4% formaldehyde, blocked with 5% BSA in PBS for 1 h, and incubated with anti-UCP1 antibody (ab10983; Abcam) and anti–firefly luciferase antibody (ab181640; Abcam) at 4°C overnight. The slides were then incubated with Alexa Fluor 647–conjugated anti-rabbit secondary antibody (ab150079; Abcam) and Alexa Fluor 488–conjugated anti-goat secondary antibody (ab150129; Abcam) at room temperature for 1 h, and the nuclei were stained with DAPI. Coverslips were imaged with a Leica microscope.

### Western Blot

Cells or various fat tissues were washed twice with ice-cold PBS, lysed with radioimmunoprecipitation assay buffer (Beyotime) for 30 min on ice, and centrifuged at 12,000*g* for 15 min at 4°C. Forty micrograms of cellular proteins or 30 μg of fat tissue proteins were resolved by 12% SDS-PAGE and transferred to polyvinylidene fluoride membrane (Millipore). Membranes were probed overnight with specific antibodies at 4°C, washed three times with Tris-buffered saline with 0.05% Tween 20, and incubated with rabbit horseradish peroxidase-conjugated secondary antibody. Membranes were developed by ECL Plus developing agent (GE Healthcare). The primary antibodies used in the experiments were antibodies to UCP1 (1:1,000, ab10983; Abcam); firefly luciferase (1:1,000, ab181640; Abcam); β-actin (1:2,000, ab8227; Abcam), P-STAT3 (1:1,000, 9145; Cell Signaling Technology), and STAT3 (1:1,000, 9132; Cell Signaling Technology).

### RNA Extraction, Reverse Transcription, and Quantitative PCR

Total RNA was isolated from cells using TRIzol Reagent (Invitrogen). First-strand cDNA synthesis was performed with Superscript III Reverse Transcriptase (Invitrogen). Quantification of mRNA levels was performed using SYBR Premix Ex Taq (Takara Bio) under optimized conditions according to the manufacturer's protocol. The reference gene used was 18S rRNA. All primers are listed in Supplementary Table 1.

### Statistical Analysis

Data are expressed as mean ± SEM. All comparisons were analyzed by unpaired two-tailed Student *t* tests. $P < 0.05$ is considered significant.

## RESULTS

### Generation of *Ucp1*-2A-Luciferase Knock-in Mice

To generate the *Ucp1*-luciferase reporter knock-in mouse, we created a construct containing the coding sequence for firefly luciferase preceded by a 2A peptide–encoding

sequence from the hand, foot, and mouth disease virus and followed by a floxed neomycin cassette. The construct was targeted to the last coding exon of the *Ucp1* gene in mouse ES, thereby replacing the endogenous *Ucp1* stop codon with the 2A peptide plus luciferase (Fig. 1*A*). The 18–amino acid 2A peptide undergoes cleavage between its COOH-terminal glycine and the N-terminal proline through a ribosomal-skipping mechanism (18). Linking proteins with 2A peptide sequences thus enables cellular expression of multiple discrete proteins in essentially equimolar quantities (19). Therefore, the resulting knock-in luciferase is brought under the control of the endogenous *Ucp1* transcriptional unit after Cre-mediated excision of the floxed neomycin gene. The correctly targeted ES clones were injected into blastocysts of 129 strain mice, and germline-transmitted mice were identified by PCR analysis (Fig. 1*B*). The expression of luciferase and cleavage of 2A peptide were validated by Western blotting (Fig. 1*C*), luciferase activity assay (Fig. 1*D*), whole-body imaging (Fig. 1*E*), and immunohistochemical analysis (Fig. 1*F*). Figure 1*C* shows that the expression of UCP1 was not compromised by insertion of the 2A-luciferase cassette. The WT mice did not express luciferase in their BAT, whereas the *Ucp1*-2A-luciferase knock-in mice had robust expression of luciferase protein with the predicted molecular mass, indicating that the 2A peptide was recognized and fully functional (Fig. 1*C*). In addition, UCP1 protein and luciferase staining patterns overlapped, suggesting that luciferase and UCP1 were colocalized (Fig. 1*F*), and the luciferase appeared active because its substrate,

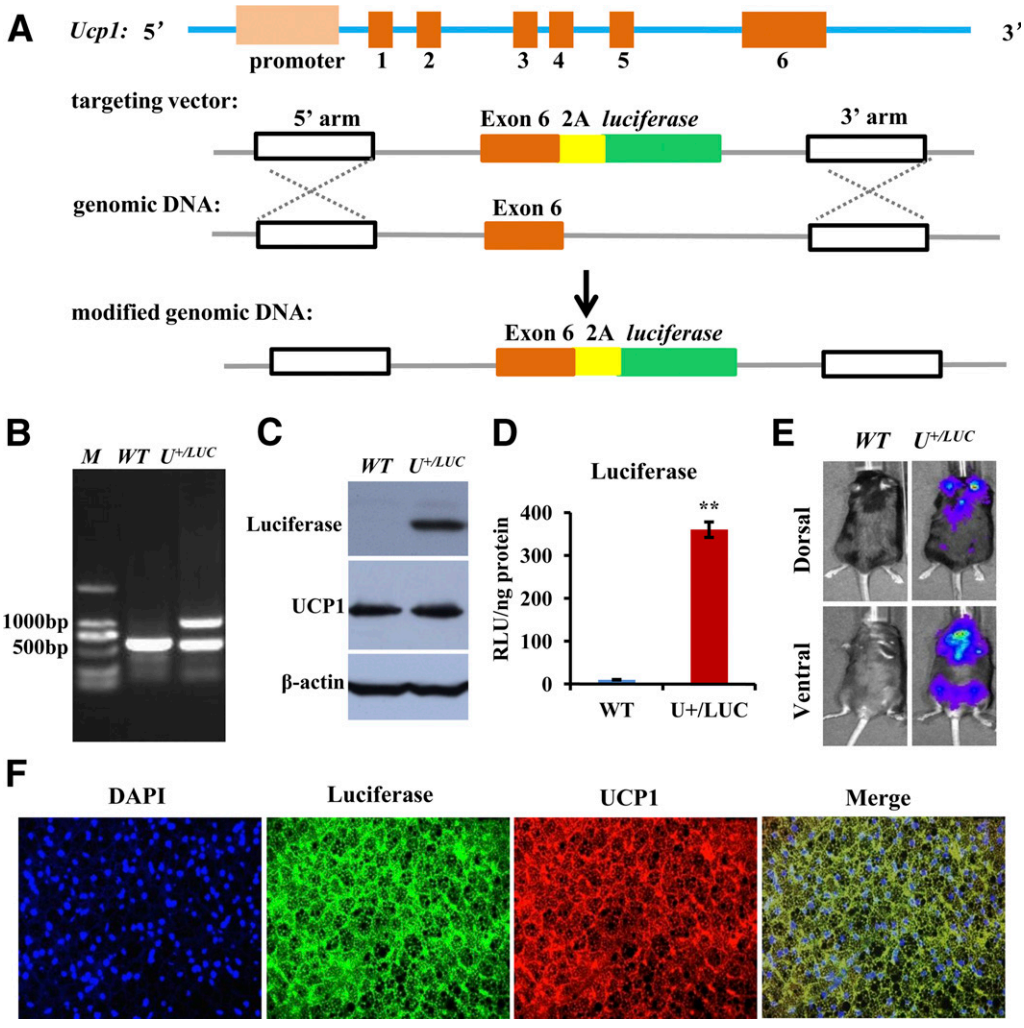


**Figure 1**—Generation and characterization of *Ucp1*-luciferase mice. *A*: Schematic of the *Ucp1*-2A-luciferase knock-in strategy showing the homologous recombination used to generate a firefly luciferase linked to a 2A peptide sequence from the hand, foot, and mouth disease virus to replace the stop codon in exon 6 of the *Ucp1* gene. *B*: Identification of luciferase knock-in mice using genomic PCR. PCR products were 500 bp for WT and 1,000 bp for *Ucp1*-2A-luciferase ($U^{+/LUC}$). *C*: UCP1 and luciferase proteins were analyzed in iBAT of WT and knock-in mice by Western blot. *D*: Luciferase enzymatic activity in iBAT of WT and luciferase knock-in mice. *E*: Whole-animal live imaging of knock-in mice showing 30-s luminescence images of *Ucp1*-2A-luciferase and WT mice. *F*: Immunohistochemical staining of UCP1 and luciferase in iBAT showing that UCP1 and luciferase immunoreactivities colocalize. $^{**}P < 0.01$. M, molecular size markers; RLU, relative light unit.

luciferin, was converted into the appropriate product with the luminescence (Fig. 1*D* and *E*).

### *Ucp1*-2A-Luciferase Recapitulates the Expression Pattern of UCP1

We tested how *Ucp1* reporter mice responded to treatment with a β3-adrenergic agonist and cold exposure. Luciferase imaging demonstrated robust signal intensification in areas corresponding to interscapular BAT (iBAT) and ingWAT (Fig. 2*A*). Similarly, the luciferase activity in mice housed at 4°C for 6 h increased significantly relative to that of mice kept at room temperature (Fig. 2*B*). Furthermore, we dissected fat pads from mice kept at room temperature (22°C) or exposed to 4°C for 12 h. Upon cold exposure, luciferase activity was greatly enhanced in the dissected fat pads, including iBAT, cervical BAT (cBAT), axiliary BAT (aBAT), and ingWAT, but not epididymal WAT (eWAT) (Fig. 2*C*). To confirm that luciferase activity reflected the expression pattern of UCP1, we compared the mRNA level of *Ucp1* and luminescence signals. The quantitative PCR (qPCR) analyses demonstrated that *Ucp1* mRNA levels mirrored luciferase activity in all fat pads (Fig. 2*D* and *E*). Furthermore, Western blot analyses revealed UCP1-positive bands only in the fat depots comprising brown or brite/beige adipocytes, including BATs and ingWAT, confirming that luciferase activity is a sensitive surrogate marker for UCP1 (Fig. 2*F* and *G*).

We subsequently performed experiments to determine the expression of luciferase and UCP1 in vivo at various time points. The relative luciferase activity, *Ucp1* mRNA, and protein expression were measured in iBAT and ingWAT after mice were kept for 0, 3, 6, 9, and 12 h at 4°C. As shown in Supplementary Fig. 1, *Ucp1* mRNA and protein expression were in concordance with luciferase activity. The fluorescence intensity was stable within 2 h by in vivo imaging. In addition, the half-lives of UCP1 and luciferase, as measured by Western blot and luciferase assay, were 10 and 5 h, respectively (Supplementary Fig. 2). In fact, expression of UCP1 and luciferase was stable and sustained in normal cells, indicating that the luciferase activity mirrors the expression of UCP1 in vivo and in vitro.

To verify the reliability of this mouse model, we examined *Ucp1* expression during interconversion of adipocytes from a white toward a brite phenotype at thermoneutrality (30°C). As shown in Supplementary Fig. 3, the expression of UCP1 in iBAT, cBAT, ingWAT, and eWAT was

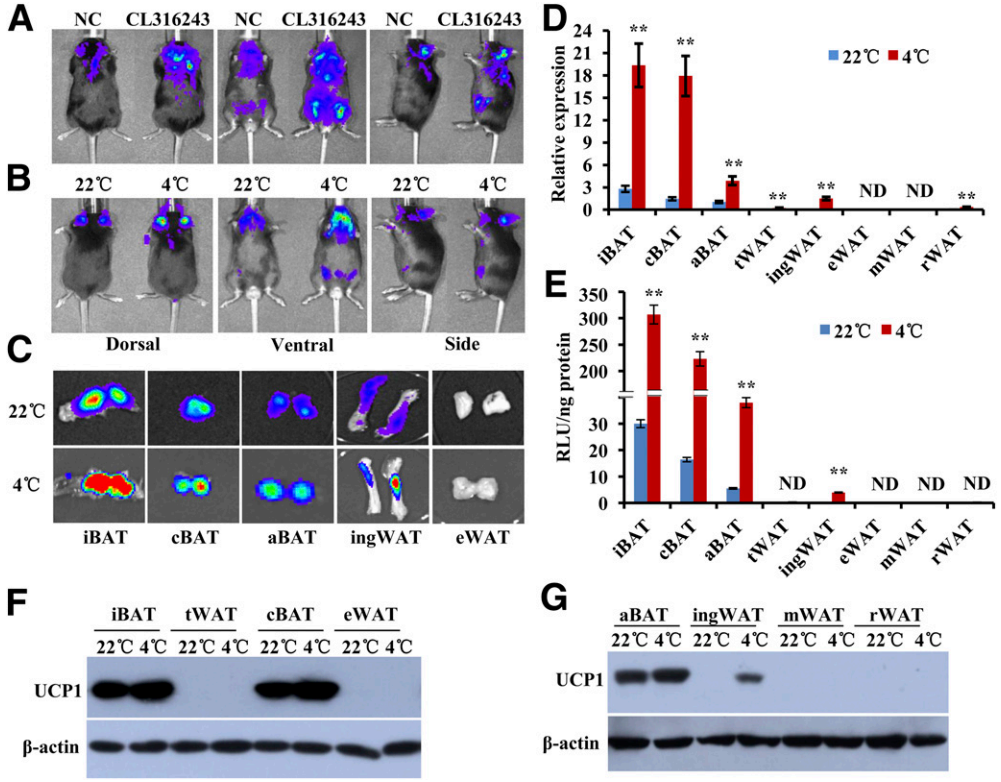


**Figure 2**—Patterns of luciferase enzymatic activity and the levels of endogenous UCP1 in adipose tissues of knock-in mice. *A* and *B*: Luminescence images of *Ucp1*-2A-luciferase mice in response to control (NC) or β3-adrenergic agonist CL316,243 (*A*) or to cold exposure (*B*). *C*: Luminescence images of adipose tissues dissected out from *Ucp1*-2A-luciferase mice in *B*. *D*: The relative levels of Ucp1 RNA in various adipose tissues of mouse measured by qPCR at 22°C and 4°C for 12 h. *E*: The relative specific luciferase activity from adipose tissues described in *D*. *F* and *G*: The protein levels of UCP1 from the adipose tissues described in *D*. $^{**}P < 0.01$, compared with control mice ($n = 5$). mWAT, mesenteric WAT; ND, not determined; RLU, relative light unit; rWAT, retroperitoneal WAT; tWAT, thoracic WAT.

increased at 4°C and decreased at 30°C. These observations support that our *Ucp1*-luciferase knock-in mouse accurately reflects UCP1 expression and thereby is a useful tool to quantify changes in UCP1 expression in vivo.

### *Ucp1*-2A-Luciferase Mice Show an Age-Dependent Decline in Luminescence

BAT helps to maintain body temperature in neonatal rodents, and its function decreases with age (20–22). To monitor UCP1 activity with age and determine a suitable age to live image browning in *Ucp1*-2A-luciferase knock-in mice, we compared mice at various ages. The live imaging intensity decreased with age, and 3-week-old mice possessed the highest UCP1 expression and luciferase activity (Fig. 3*A–E*).

### Identification of a Novel Beige/BAT Fat Depot Underneath the Ears

By detecting the *Ucp1*-driven luciferase activity, we identified a novel fat depot underneath the ears that exhibited strong luciferase activity, which we named uBAT (underneath ear BAT). As illustrated in Figs. 1*E*, 2*A*, and 3*A*, the luciferase imaging intensity was highly concentrated around the ears and further enhanced upon exposure to cold or treatment with a β3-adrenergic agonist. To characterize the precise anatomical location of uBAT, we dissected sample tissues from this area and subjected them to immunohistochemical and molecular analyses. As shown in Fig. 4*A–C*, the positive tissue was not the ears per se, but a diffuse fat pad underneath the ears. The H-E histological staining showed that the fat pad contained both unilocular and multilocular adipocytes at room temperature (Fig. 4*D*). Moreover, the expression of Ucp1 was readily detected in the multilocular adipocytes, even at room temperature, and the percentage of these UCP1-positive multilocular adipocytes was further increased upon cold exposure (Fig. 4*E*). This observation was consistent with the results from the luciferase assay, which showed that the luciferase activity of uBAT was ~25% of that in iBAT and 10-fold of that in ingWAT (Fig. 4*E*). After cold exposure, the luciferase activity was further increased (by 3.5-fold) to levels comparable with iBAT at room temperature (Fig. 4*E*). The levels of brown- and beige-related gene expression in uBAT were also examined by qPCR. Similar to ingWAT and iBAT, expression of the brown-related genes, including *Ucp1*, *Prdm16*, and *Cidea*, was significantly induced in uBAT in response to cold exposure (Fig. 4*F–H*). To determine whether uBAT comprises classic brown or beige adipocytes in nature, we compared the expression of markers for these two adipocytes. The markers for beige adipocytes, including *Tbx1*, *Tmem26*, *Cd137*, and *Hoxc9*, were expressed at levels comparable with ingWAT (Fig. 4*F–H*) and were further induced in uBAT. In contrast, *Zic1*, a marker for classic brown adipocytes (23,24), was detected in uBAT and induced ~3.5-fold during cold exposure (Fig. 4*F–H*). Compared with iBAT and ingWAT, the expression pattern of uBAT was amid iBAT and ingWAT. We also examined UCP1 expression at thermoneutrality (30°C) and compared it with that at 4°C and 22°C. As shown in Supplementary Fig. 3*A* and *E*, the expression of UCP1 in uBAT was increased at 4°C and decreased at 30°C. Taken together, these results strongly suggest that the UCP1-positive cells in uBAT represent a mixture of beige adipocytes and the classic brown adipocytes present in iBAT.

### *Ucp1*-2A-Luciferase System Is a Convenient Reporter Model for Drug Screening

The possibility of using primary cells from these mice as a screening platform to obtain compounds or peptides with browning capacity was also explored. To this end, we isolated and differentiated the preadipocytes from

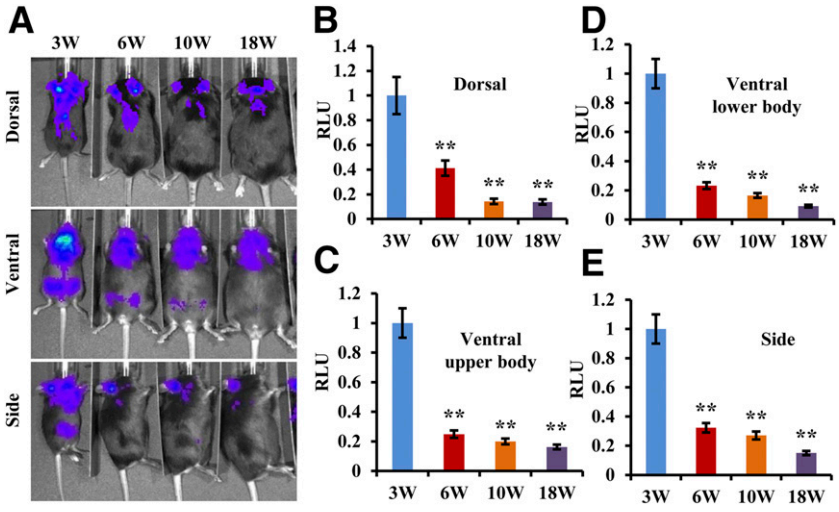


**Figure 3**—Declined luciferase activity supports that browning ability decreases with age. *A*: Luminescence images of *Ucp1*-2A-luciferase mice at age 3, 6, 10, and 18 weeks at 22°C. *B–E*: Quantification of luminescence in *A* for the dorsal, ventral upper body, ventral lower body, and side view images at age 3, 6, 10, and 18 weeks at 22°C. $^{**}P < 0.01$, compared with mice from the control group ($n = 5$). RLU, relative light unit; W, week.

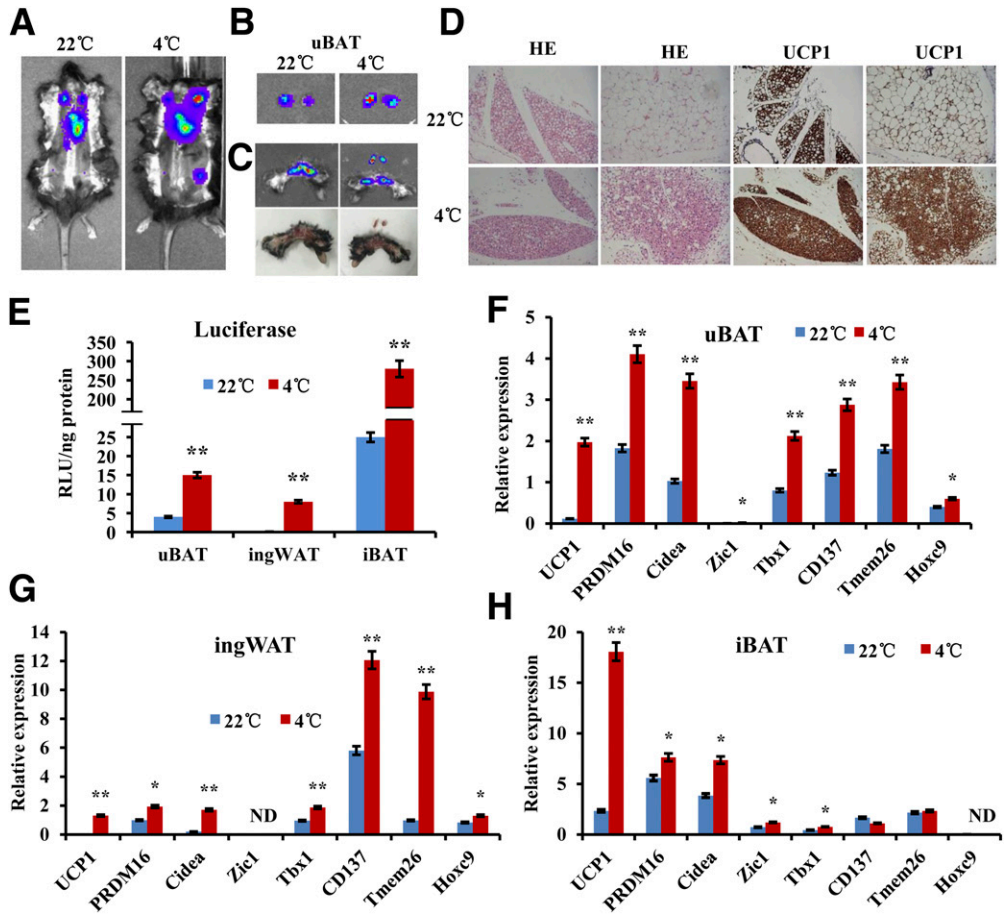


**Figure 4**—uBAT was revealed by live imaging of *Ucp1*-2A-luciferase knock-in mice. *A*: Luminescence images of a *Ucp1*-2A-luciferase mouse at 22°C and 4°C for 12 h. *B*: Luminescence images of the region containing uBAT in a *Ucp1*-2A-luciferase mouse at 22°C and 4°C for 12 h. *C*: Ears and attached uBAT. *D*: H-E and immunohistochemical staining of UCP1 in uBAT, showing both classic BAT and beige adipose tissue. *E*: Relative specific luciferase activity in uBAT, ingWAT, and iBAT after *Ucp1*-2A-luciferase mice were kept at 22°C and 4°C for 12 h. *F–H*: Relative expression of *Ucp1*, *Prdm16*, *Cidea*, *Zic1*, *Tbx1*, *Cd137*, *Tmem26*, and *Hoxc9* mRNAs in uBAT, ingWAT, and iBAT after *Ucp1*-2A-luciferase mice were kept at 22°C and 4°C for 12 h. $^*P < 0.05$, $^{**}P < 0.01$, compared with controls ($n = 5$). ND, not determined; RLU, relative light unit.

ingWAT in vitro. To validate the screening platform, several known browning agents were tested, including the β3-adrenergic receptor agonist CL316,243, FGF21 (8), the AMPK agonist A-769662 (25), the peroxisome proliferator–activator receptor γ activator fmoc-Leu-OH (26), β-aminoisobutyric acid (BAIBA) (27), all-*trans* retinoic acid (ATRA), and the synthetic retinoic acid analog AM580. These agents increase energy expenditure and/or alleviate insulin resistance in obese mouse models (28–30). Two screening strategies were adopted: Test compounds were either present during the entire differentiation period or added to mature adipocytes during the final 2 days of differentiation (Fig. 5*A*). When the compounds were included during the entire differentiation process, all compounds, except BAIBA, significantly increased luminescence (Fig. 5*A*), suggesting that they promote differentiation of beige precursor cells or possess browning activities. More importantly, adding them to mature adipocytes also increased luminescence significantly (Fig. 5*A*). Specifically, we found that both ATRA and AM580 increased luciferase activity in a dose-dependent manner (Fig. 5*B–D*).

### Axitinib Increases UCP1 Expression and Thermogenesis in *Ucp1*-2A-Luciferase Mice

With our luciferase reporter system, we found that axitinib, a potent inhibitor of vascular endothelial growth factor (VEGF) receptors (31), had potential browning activity (Fig. 6*A*). In contrast, other tyrosine kinase inhibitors, including cediranib, masitinib, tandutinib, and BIBF1120, did not show a browning effect (Fig. 6*A*). The effect of axitinib on induction of both luciferase and *Ucp1* expression was dose dependent (Fig. 6*B* and *C*). Of note, enhanced expression of *Ucp1* by axitinib was suppressed by activation of STAT3 with the STAT3-specific activator SD19 (Fig. 6*D*), suggesting that the STAT3 pathway inhibits axitinib-induced *Ucp1* expression. Consistent with this finding, we observed reduced

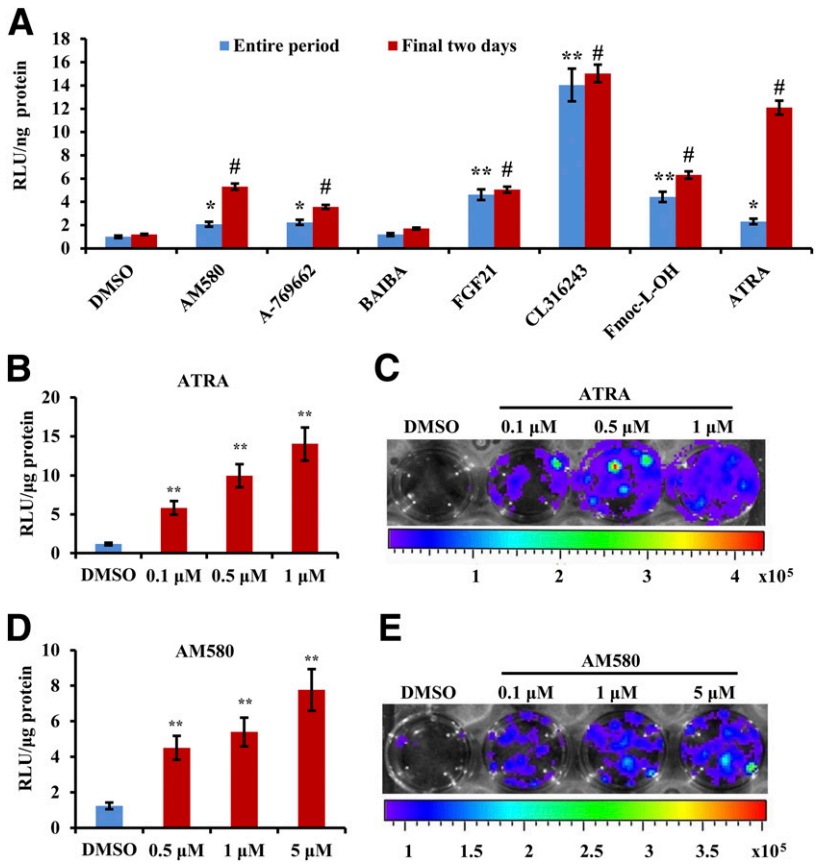


**Figure 5—** Drug screening in white adipocytes from *Ucp1*-2A-luciferase knock-in mice. *A*: Relative browning induced by selected molecules (1 μmol/L) during the entire period (days 0–10) and during the final 2 days (days 8–10) of in vitro adipocyte differentiation of primary inguinal preadipocytes. *B*: Relative luciferase activities in response to various concentrations of ATRA. *C*: Luminescence images of luciferase activities in response to various concentrations of ATRA. *D*: Relative luciferase activities in response to various concentrations of AM580. *E*: Luminescence images of luciferase activities in response to various concentrations of AM580. #$P < 0.05$, final 2 days groups compared with control group; *$P < 0.05$, **$P < 0.01$, compared with control group ($n = 5$). RLU, relative light unit.

phosphorylation of STAT3 in cells treated with axitinib (Fig. 6*E* and *F*).

The browning activity of axitinib was further tested in vivo. Accordingly, *Ucp1*-2A-luciferase mice were treated with vehicle or axitinib for 8 weeks along with an HFD. We found that mice receiving axitinib gained less weight than those receiving vehicle control (Fig. 7*F*). Axitinib-treated mice also exhibited improved glucose disposal ability as determined by glucose and insulin tolerance tests (Fig. 7*G* and *H*). H-E staining showed that axitinib-treated mice had smaller adipocytes than control mice (Fig. 7*K*). In addition, the symptom of fatty liver was also alleviated by axitinib treatment (Fig. 7*L*). Consistent with these observations, the fat mass and weight of ingWAT, eWAT, and liver were lower in axitinib-treated mice (Fig. 7*I*). Furthermore, in vivo luciferase imaging showed a marked increase in luciferase activities in the iBAT, ingWAT, and uBAT of the *Ucp1*-2A-luciferase reporter mice administered axitinib (Fig. 7*A*–*E*). The luciferase activities in iBAT, ingWAT, and eWAT were elevated in these mice as well (Fig. 7*J*). $O_2$ consumption, $CO_2$ production (Supplementary Fig. 4*A*–*C*), and rectal temperature (Supplementary Fig. 4*D*) were significantly increased by axitinib, suggesting an increased energy expenditure without much difference in food intake and activity (Supplementary Fig. 4*E* and *G*). We did not observed an increased heart rate or increased blood pressure (Supplementary Fig. 4*H*–*J*), indicating that axitinib did not cause a general sympathetic activation. A selective activation to adipose tissues cannot be excluded at this point. However, by using the Seahorse bioanalyzer, we demonstrated that axitinib increased OCRs under various respiration situations in cultured adipocytes (Supplementary Fig. 4*K* and *L*), indicating an increased mitochondrial content of the treated cells. Taken together, these results indicate that axitinib can directly increase respiratory capacity in adipocytes and, thus, may represent a novel browning agent.

## DISCUSSION

The 2A peptide sequences from the picornavirus family share a highly conserved motif of an 18–amino acid sequence, mediating the cleavage between the COOH-terminal

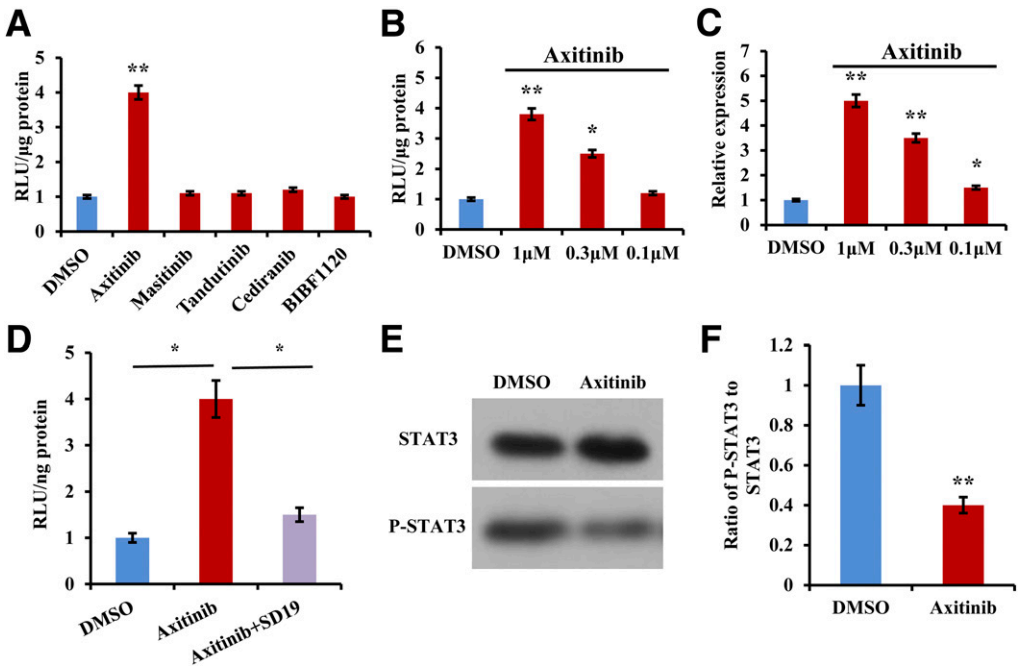


**Figure 6**—Axitinib increases browning in ingWAT. *A*: Relative browning induced by selected tyrosine kinase inhibitors (1 μmol/L) in primary ingWAT. *B*: Relative luciferase activities in response to various concentrations of axitinib. *C*: Relative mRNA expression in response to various concentrations of axitinib. *D*: STAT3 suppresses the UCP1 mRNA expression induced by axitinib. *E* and *F*: Phosphorylation of STAT3 was reduced in cells treated with axitinib. STAT3 was activated by the specific activator SD19. $^{*}P < 0.05$, $^{**}P < 0.01$, compared with DMSO ($n = 5$). RLU, relative light unit.

glycine and the N-terminal proline of the 2A sequence (18). In our mouse model, 2A peptide left a proline on the N terminus of luciferase but did not affect the luciferase activity, which we demonstrated in a previous study (32). The functionality of luciferase is also corroborated by the readily detectable luminescence in our mouse model. Recognition and processing of the 2A peptide also created a COOH-terminal 20–amino acid tag on UCP1 with a sequence of GSGATNFSLLKQAGDVEENPG (where GSG is a flexible linker between UCP1 and the 2A peptide), but this C terminus does not appear to abolish the biological function of UCP1 because the homozygous mice behave normally like WT mice when exposed to cold temperature, which is in contrast to *Ucp1* null mutants (data not shown). Of note, we did not observe a mobility shift with heterozygous or homozygous mice compared with WT mice in terms of UCP1 immunoreactive bands under 10–15% SDS-PAGE (Fig. 1*C* and data not shown). A similar observation was published in a previous study (33).

Through our UCP1-luciferase knock-in mice, we discovered an area underneath the ears that exhibited strong UCP1 induction in response to cold or β3-adrenergic agonist, with expression patterns of both brown and beige adipocytes. Currently, the biological function of such an adipose depot is elusive. Its small size presumably precludes it from being metabolically significant; however, sensitive response to temperature changes and/or adrenergic stimuli may prove important for an organism to rapidly prepare for and adapt to changes internally and externally.

During the final stages of this study, Galmozzi et al. (12) reported their generation of a *Ucp1*-luciferase reporter mouse line using bacterial artificial chromosome transgenic techniques. The segregation pattern indicated that they inserted the transgene into the Y chromosome. In contrast, we inserted the luciferase coding sequence into exon 6 of the *Ucp1* gene, thereby integrating the luciferase reporter into a genomic location that promoted the expression of the UCP1-luciferase fusion protein in the same location as endogenous UCP1. Our *Ucp1*-2A-luciferase reporter mouse model is a highly reproducible platform for screening browning compounds. Except for known UCP1-activating agents, a previously unrecognized compound, axitinib, an inhibitor of the VEGF receptor, has been identified. Of note, other VEGF receptor targeting drugs do not have an effect on browning (Fig. 6*A*), suggesting that axitinib induces browning independent of the VEGF receptor. Axitinib possibly enhances UCP1 expression through inhibiting the STAT3 pathway. This is supported by a recent report that the Janus kinase/STAT pathway regulates the metabolic conversion of white adipocytes to brown adipocytes in humans (34). Furthermore, as shown in the current study, axitinib treatment enhanced $O_2$ consumption and rectal temperature. Thus, axitinib treatment decreased body weight gain and fat accumulation by increasing

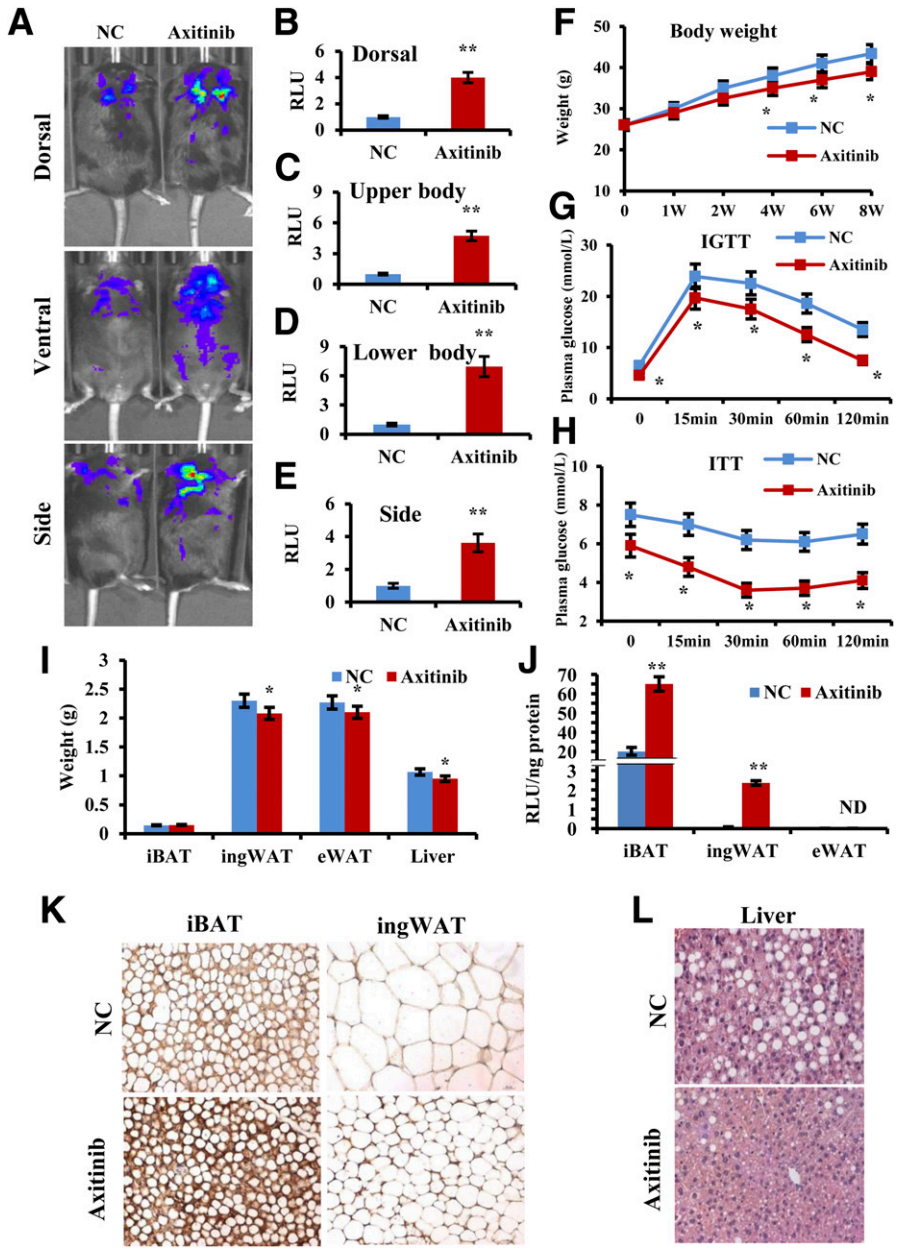


**Figure 7**—Axitinib increases thermogenesis in vivo. *A*: Live visualization and quantification of luciferase activity in *Ucp1*-2A-luciferase mice treated with vehicle or axitinib for 8 weeks. Representative mice are shown. *B–E*: Quantification of luminescence in *A* for the dorsal, ventral upper body, ventral lower body, and side view images. *F*: Axitinib limited body weight gain in *Ucp1*-2A-luciferase mice fed an HFD. *G* and *H*: Axitinib improved glucose clearance in *Ucp1*-2A-luciferase mice ($n$ = 9). *I*: Axitinib reduced the weight of ingWAT, eWAT, and liver in *Ucp1*-2A-luciferase mice. *J*: Relative luciferase activities in response to axitinib showed enhanced *Ucp1* expression. *K*: UCP1 immunostaining in iBAT and ingWAT from *Ucp1*-2A-luciferase mice fed an HFD treated with vehicle or axitinib. *L*: H-E staining of fatty liver from mice treated with vehicle or axitinib. *$P$ < 0.05, **$P$ < 0.01, compared with control group ($n$ = 9). IGTT, intraperitoneal glucose tolerance test; ITT, insulin tolerance test; NC, nontreated control; ND, not determined; RLU, relative light unit; W, week.

energy expenditure and enhancing thermogenesis. Moreover, we did not observe significant differences in food intake between the two groups of mice, which is consistent with previous reports in animals (35), although loss of appetite has been reported as a possible adverse effect of axitinib in humans. Axitinib still has several advantages over other drugs, including its favorable profile of toxicity and that it can be administered on a constant and manageable schedule with limited toxicity (36). Thus, axitinib may be an effective drug for treating metabolic disease.

In summary, our study establishes a sensitive, noninvasive, and convenient system to monitor UCP1 function, which can be used to screen drugs and help to

identify and validate compounds with browning effects in vitro and in vivo.

**Funding.** This work was partially supported by funds from the National Basic Research Program of China (2016YFC1305000, 2010CB945500, and 2011CB504004), an international collaborative fund from the Chinese Academy of Sciences (154144KYSB20150019), Guangdong Province (2015A05050241 and 2014A010107024), the Guangzhou Municipal Bureau of Science and Technology (2016201604030030), and the National Science Foundation of China (81327801 and 31301019). K.K. was supported by the Danish Natural Science Research Council, the Novo Nordisk Foundation, and the Carlsberg Foundation.

**Duality of Interest.** No potential conflicts of interest relevant to this article were reported.

**Author Contributions.** L. Mao, B.N., and D.W. researched data and contributed to the writing of the manuscript. L. Mao, T.N., and K.L. contributed to the generation of the *Ucp1*-2A-luciferase mouse model. L. Mao performed the Western blot analyses, histological experiments, immunostaining, luciferase imaging, and luminescence activity. L. Mao, X.T., and R.Y. performed mRNA expression. L. Mao, T.N., X.H., X. Lin, Y.X., and Z.Z. performed the energy expenditure experiments, Seahorse analysis, and blood pressure and heart beat measurements. T.N., X.H., X.G., X. Liu, P. Li, K.D., Y.W., A.X., W.H., P. Liu, and S.D. reviewed the manuscript and contributed to the discussion. T.N., J.F., S.D., and D.W. conceived the research ideas and reviewed and edited the manuscript. X.H. and K.K. reviewed and edited the manuscript. L.Mad., S.D., and D.W. conceived the research ideas and supervised the project. L.Mad. and S.D. contributed to the writing of the manuscript. D.W. is the guarantor of this work and, as such, had full access to all the data in the study and takes responsibility for the integrity of the data and the accuracy of the data analysis.

## References

1. Cypess AM, Lehman S, Williams G, et al. Identification and importance of brown adipose tissue in adult humans. N Engl J Med 2009;360:1509–1517
2. van Marken Lichtenbelt WD, Vanhommerig JW, Smulders NM, et al. Cold-activated brown adipose tissue in healthy men. N Engl J Med 2009;360:1500–1508
3. Virtanen KA, Lidell ME, Orava J, et al. Functional brown adipose tissue in healthy adults. N Engl J Med 2009;360:1518–1525
4. Cypess AM, Weiner LS, Roberts-Toler C, et al. Activation of human brown adipose tissue by a β3-adrenergic receptor agonist. Cell Metab 2015;21:33–38
5. Bartelt A, Bruns OT, Reimer R, et al. Brown adipose tissue activity controls triglyceride clearance. Nat Med 2011;17:200–205
6. Stanford KI, Middelbeek RJ, Townsend KL, et al. Brown adipose tissue regulates glucose homeostasis and insulin sensitivity. J Clin Invest 2013;123:215–223
7. Liu X, Zheng Z, Zhu X, et al. Brown adipose tissue transplantation improves whole-body energy metabolism. Cell Res 2013;23:851–854
8. Fisher FM, Kleiner S, Douris N, et al. FGF21 regulates PGC-1α and browning of white adipose tissues in adaptive thermogenesis. Genes Dev 2012;26:271–281
9. Gnad T, Scheibler S, von Kügelgen I, et al. Adenosine activates brown adipose tissue and recruits beige adipocytes via A2A receptors. Nature 2014;516:395–399
10. Zhang Z, Zhang H, Li B, et al. Berberine activates thermogenesis in white and brown adipose tissue. Nat Commun 2014;5:5493
11. Rosenwald M, Perdikari A, Rülicke T, Wolfrum C. Bi-directional interconversion of brite and white adipocytes. Nat Cell Biol 2013;15:659–667
12. Galmozzi A, Sonne SB, Altshuler-Keylin S, et al. ThermoMouse: an in vivo model to identify modulators of UCP1 expression in brown adipose tissue. Cell Reports 2014;9:1584–1593
13. Ohlson KB, Shabalina IG, Lennström K, et al. Inhibitory effects of halothane on the thermogenic pathway in brown adipocytes: localization to adenylyl cyclase and mitochondrial fatty acid oxidation. Biochem Pharmacol 2004;68:463–477
14. Matsumoto T, Kano K, Kondo D, et al. Mature adipocyte-derived dedifferentiated fat cells exhibit multilineage potential. J Cell Physiol 2008;215:210–222
15. Fasshauer M, Klein J, Kriauciunas KM, Ueki K, Benito M, Kahn CR. Essential role of insulin receptor substrate 1 in differentiation of brown adipocytes. Mol Cell Biol 2001;21:319–329
16. Matthias A, Ohlson KB, Fredriksson JM, Jacobsson A, Nedergaard J, Cannon B. Thermogenic responses in brown fat cells are fully UCP1-dependent. UCP2 or UCP3 do not substitute for UCP1 in adrenergically or fatty acid-induced thermogenesis. J Biol Chem 2000;275:25073–25081
17. Li Y, Fromme T, Schweizer S, Schöttl T, Klingenspor M. Taking control over intracellular fatty acid levels is essential for the analysis of thermogenic function in cultured primary brown and brite/beige adipocytes. EMBO Rep 2014;15:1069–1076
18. Donnelly ML, Luke G, Mehrotra A, et al. Analysis of the aphthovirus 2A/2B polyprotein 'cleavage' mechanism indicates not a proteolytic reaction, but a novel translational effect: a putative ribosomal 'skip'. J Gen Virol 2001;82:1013–1025
19. de Felipe P, Luke GA, Hughes LE, Gani D, Halpin C, Ryan MD. E unum pluribus: multiple proteins from a self-processing polyprotein. Trends Biotechnol 2006;24:68–75
20. Rogers NH, Landa A, Park S, Smith RG. Aging leads to a programmed loss of brown adipocytes in murine subcutaneous white adipose tissue. Aging Cell 2012;11:1074–1083
21. Mattson MP. Perspective: does brown fat protect against diseases of aging? Ageing Res Rev 2010;9:69–76
22. Ma X, Lin L, Qin G, et al. Ablations of ghrelin and ghrelin receptor exhibit differential metabolic phenotypes and thermogenic capacity during aging. PLoS One 2011;6:e16391
23. Jespersen NZ, Larsen TJ, Peijs L, et al. A classical brown adipose tissue mRNA signature partly overlaps with brite in the supraclavicular region of adult humans. Cell Metab 2013;17:798–805
24. Waldén TB, Hansen IR, Timmons JA, Cannon B, Nedergaard J. Recruited vs. nonrecruited molecular signatures of brown, "brite," and white adipose tissues. Am J Physiol Endocrinol Metab 2012;302:E19–E31
25. Cool B, Zinker B, Chiou W, et al. Identification and characterization of a small molecule AMPK activator that treats key components of type 2 diabetes and the metabolic syndrome. Cell Metab 2006;3:403–416
26. Rocchi S, Picard F, Vamecq J, et al. A unique PPARgamma ligand with potent insulin-sensitizing yet weak adipogenic activity. Mol Cell 2001;8:737–747
27. Roberts LD, Boström P, O'Sullivan JF, et al. β-Aminoisobutyric acid induces browning of white fat and hepatic β-oxidation and is inversely correlated with cardiometabolic risk factors. Cell Metab 2014;19:96–108
28. Tsuchiya H, Ikeda Y, Ebata Y, et al. Retinoids ameliorate insulin resistance in a leptin-dependent manner in mice. Hepatology 2012;56:1319–1330
29. Guleria RS, Singh AB, Nizamutdinova IT, et al. Activation of retinoid receptor-mediated signaling ameliorates diabetes-induced cardiac dysfunction in Zucker diabetic rats. J Mol Cell Cardiol 2013;57:106–118
30. Ghorbani M, Shafiee Ardestani M, Gigloo SH, Cohan RA, Inanlou DN, Ghorbani P. Anti diabetic effect of CL 316,243 (a β3-adrenergic agonist) by down regulation of tumour necrosis factor (TNF-α) expression. PLoS One 2012;7:e45874
31. Pithavala YK, Chen Y, Toh M, et al. Evaluation of the effect of food on the pharmacokinetics of axitinib in healthy volunteers. Cancer Chemother Pharmacol 2012;70:103–112
32. Yang S, Kuang Y, Li H, et al. Enhanced production of recombinant secretory proteins in *Pichia pastoris* by optimizing Kex2 P1′ site. PLoS One 2013;8:e75347
33. Ryan MD, Drew J. Foot-and-mouth disease virus 2A oligopeptide mediated cleavage of an artificial polyprotein. EMBO J 1994;13:928–933
34. Moisan A, Lee YK, Zhang JD, et al. White-to-brown metabolic conversion of human adipocytes by JAK inhibition. Nat Cell Biol 2015;17:57–67
35. Langlet F, Levin BE, Luquet S, et al. Tanycytic VEGF-A boosts blood-hypothalamus barrier plasticity and access of metabolic signals to the arcuate nucleus in response to fasting. Cell Metab 2013;17:607–617
36. Kelly RJ, Rixe O. Axitinib—a selective inhibitor of the vascular endothelial growth factor (VEGF) receptor. Target Oncol 2009;4:297–305